2013

Calculated Vibrational Properties of Ubisemiquinones

Hari P. Lamichhane

Gary Hastings
Georgia State University, ghastings@gsu.edu

Recommended Citation

Lamichhane, H. & and Hastings, G. (2013). Calculated Vibrational Properties of Ubisemiquinones. *Computational Biology Journal,* Article ID 807592, 1-11. doi: 10.1155/2013/807592

Hindawi Publishing Corporation
Computational Biology Journal
Volume 2013, Article ID 807592, 11 pages
http://dx.doi.org/10.1155/2013/807592

Research Article

Calculated Vibrational Properties of Ubisemiquinones

Hari P. Lamichhane and Gary Hastings

Department of Physics and Astronomy, Georgia State University, 29 Peachtree Center Avenue, Atlanta, GA 30303, USA

Correspondence should be addressed to Gary Hastings; ghastings@gsu.edu

Received 15 October 2012; Accepted 27 November 2012

Academic Editor: Philip Crooke

Density functional theory has been used to calculate harmonic normal mode vibrational frequencies for unlabeled and isotope-labeled ubisemiquinones in both the gas phase and in several solvents. It is shown that four methoxy group conformations are likely to be present in solution at room temperature. Boltzmann weighted infrared and Raman spectra for the four conformers were calculated, and composite spectra that are the sum of the Boltzmann weighted spectra were produced. These composite spectra were compared to experimental FTIR and resonance Raman spectra, and it is shown that the calculated band frequencies, relative band intensities, and ^{13}C and ^{18}O isotope-induced band shifts are in excellent agreement with experiment. The calculations show that the C=O and C=C modes of ubisemiquinone strongly mix with methoxy methyl CH bending vibrations, and that the degree of mixing is altered upon isotope labeling, resulting in complicated changes in mode frequencies, intensities, and composition upon isotope labeling. Upon consideration of the calculated potential energy distributions of the normal modes of ubisemiquinone, and how they change upon isotope labeling, an explanation of some puzzling features in previously published Raman spectra is provided.

1. Introduction

Ubiquinones (UQ_n: 2,3-dimethoxy-5-methyl-6-polyprenyl-1,4-benzoquinones) play an important role in biological electron and proton transfer processes that occur in both respiration and photosynthesis [1]. In photosynthetic reaction centers from purple bacteria, two UQ molecules, called Q_A and Q_B, act as terminal electron acceptors [2]. In purple bacterial reaction centers (PBRCs) (see Abbreviations) from *Rhodobacter* (*Rb.*) *sphaeroides*, Q_A and Q_B are both ubiquinone-10 (UQ_{10}) molecules. Q_A and Q_B have very different functions; however, Q_A is an intermediary cofactor involved in transferring electrons from bacteriopheophytin to Q_B, while Q_B couples electron and proton transfer processes [3, 4]. The very different redox functions of Q_A and Q_B are testimony to the flexibility of UQs in biological processes. Since Q_A and Q_B are both UQ_{10} molecules, pigment-protein interactions must modulate the functional properties of UQ_{10} in PBRCs. Elucidation of these pigment-protein interactions is at the heart of much current research in photosynthesis [5, 6].

Fourier transform infrared (FTIR) difference spectroscopy (DS) is a sensitive molecular-level probe of pigment-protein interactions, and it is widely used to study both the neutral and reduced states of the quinones occupying the Q_A and Q_B binding sites in PBRCs [7]. Although Q_A^-/Q_A and Q_B^-/Q_B FTIR difference spectra have been obtained under a wide range of conditions for variously treated PBRC's, these spectra continue to be difficult to interpret because many bands not associated with the quinone also contribute to the spectra. Reconstitution of PBRCs with isotopically labeled quinones, however, has allowed some separation of the contributions of the quinones from those of the protein to the spectra [7]. Nonetheless the hypothesized band assignments in the experimental spectra, particularly those assignments associated with the ubiquinone anion radical, are still ambiguous and have not been modeled computationally.

One basis for developing an understanding of bands in Q_A^-/Q_A and Q_B^-/Q_B FTIR DS is to first consider spectra of the relevant quinones in solution. Infrared (IR) absorption spectra [8, 9] and resonance Raman spectra [10] for

ubisemiquinones in solution have been obtained. However, from a computational standpoint, even these simpler solution spectra are poorly understood. The work outlined in this paper is aimed at addressing this problem.

Few computational studies aimed at modeling the vibrational properties of ubisemiquinones (UQ^-) have been undertaken. The work that has been undertaken [11, 12] is limited in one way or another; for example, tail-less quinone models in only the gas phase were considered, using relatively low levels of theory. Previously it was claimed that the calculated normal modes and associated isotope-induced frequency shifts are in good agreement with experiment [12]. Isotope shifts do appear to agree with experiment. However, upon careful examination, it appears that the previously calculated normal modes (frequencies and intensities) are *not* in agreement with experimental spectra (see below). In the light of this finding we have used more robust computational methods to investigate the vibrational properties of ubisemiquinones in the gas phase and in solution.

In this paper we describe the simulation of FTIR and Raman spectra associated with labeled and unlabeled tail-containing ubisemiquinones in both the gas phase and in solvent.

2. Materials and Methods

2.1. Calculations. Molecular geometry optimizations and harmonic vibrational frequency calculations were performed using hybrid density functional theory (DFT) methods, employing the B3LYP functional and the 6-31 + G(d) basis set within Gaussian 03 [13]. 6-31 + G(d) is preferable to 6-31 G(d) for calculations involving semiquinones [14]. For calculations including solvent, the integral equation formalism (IEF) [15–17] of the polarizable continuum model (PCM) [18, 19] was used. The PCM uses the united atom cavity approach. Cavity parameters used were OFac = 0.89 (overlap index between interlocking spheres) and $R_{\text{Min}} = 0.2$ (minimum radius in Angstroms for overlapping spheres). Very similar spectra were calculated when a smaller number of added spheres were considered (OFac = 0.8 and $R_{\text{Min}} = 0.5$). The potential energy distribution (PED) (or total energy distribution) of normal modes was calculated using gar2ped [20].

Calculated normal mode vibrational frequencies presented here were scaled by 0.9808. Such a scale factor is standard for calculations using the specified functional and basis set and was derived by comparing the frequencies of bands in experimental and calculated spectra. Such a scaling of the calculated frequencies is undertaken only to facilitate a comparison between calculated and experimental spectra. We are primarily interested in vibrational frequency changes that occur upon isotope labeling, and these frequency differences are accurately calculated without scaling [14, 21].

3. Results

3.1. UQ Structure and Numbering. Figure 1 shows a geometry-optimized UQ_1^- model with the atom numbering scheme displayed. UQ has two carbonyl groups (C_1=O_{18} and C_4=O_{15}), two methoxy groups (C_3–O_{16}–CH_3 and C_2–O_{17}–CH_3), a methyl group at C_5, and an isoprene unit at C_6. In our calculations we used UQ models with only a single isoprene unit. As outlined previously [21], the calculated vibrational properties of UQ_1 (or UQ_1^-) are very similar to that found for UQ_n (with $n > 1$). Also shown in Figure 1 are relevant internal coordinates of UQ_1^-. The normal modes will be expressed in terms of contributions from these internal coordinates. Of particular interest in this paper are the coordinates R3, R9, R4, and R10 which are due to $C_1\cdots O$, $C_4\cdots O$, $C_2\cdots C_3$, and $C_5\cdots C_6$ stretching vibrations, respectively. The methoxy methyl CH bending vibrations (coordinates δC8 and δC9) are also of considerable relevance in this paper, as they strongly couple to the C$\cdots$O vibrations (see below). This was not found to occur for neutral UQ [21].

3.2. Calculated Structure of Ubisemiquinone$_1$ (UQ_1^-). Previously we showed that neutral UQ_1 can adopt at least eight different methoxy group conformations at room temperature [21]. To establish which conformations may be present for UQ_1^-, single-point energy calculations were undertaken for methoxy group dihedral angles that were stepped in 10° increments. That is, 36 × 36 structures with fixed methoxy group dihedral angles were geometry optimized.

A contour plot of energy versus the C_2 and C_3 dihedral angles is shown in Figure 2, which indicates that there are four low-energy UQ_1^- conformations, each with C_2 and C_3 dihedral angles close to ±120°. The four conformers are labeled A, B, E, and F in Figure 2. These four conformers are similar to the neutral UQ_1 conformers labeled J, L, I, and K, respectively, that were described previously [21].

Following single-point energy calculations, the four UQ_1^- conformations were further geometry optimized (energy minimized) without constraining the dihedral angles. Calculations were undertaken for the four conformations in the gas phase and in several solvents that have dielectric constants spanning a wide range (2.2–78).

Calculated bond lengths, the C_6–C_{10}–C_{11} bond angle, and methoxy group dihedral angles for the various UQ_1^- conformers in the gas phase and CCl_4 are listed in Table 1. Similar trends in the listed data are calculated for the conformers in other solvents (data not shown). Data for UQ_{10}/UQ_{10}^- in the Q_A/Q_B binding site is also listed in Table 1.

The data presented in Table 1 demonstrates that all four conformers in solvent are within 0.45 kcal/mol in energy (kT at 298 K is ~0.59 kcal/mol), so all four conformers would be expected to be present to some degree in solvent at room temperature. The orientation of the methoxy groups of the four geometry-optimized conformers (in CCl_4) as well as the calculated dihedral angles are shown in the insets in Figure 2. The corresponding dihedral angles for the four conformers in different solvents are similar (data not shown).

The hydrocarbon chain (isoprene unit) attached at C_6 makes a distinct kink at C_{10}. The C_6–C_{10}–C_{11} angle is close to 113° for all four conformers (Table 1). This angle is also

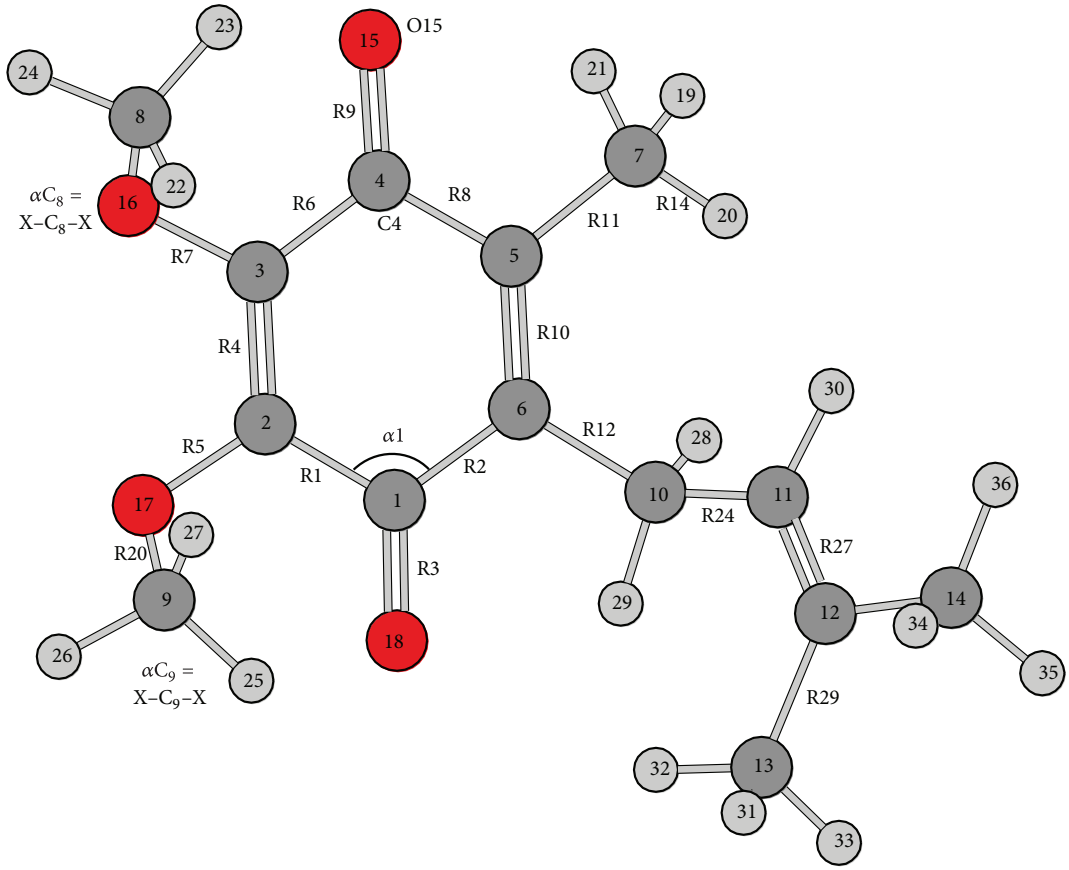

Figure 1: Structure and atomic numbering scheme for an optimized UQ_1^- model. Various internal coordinates are also outlined. R represents bond stretching, α represents a bending of the angle between two bonds, and δ represents a combination of angle bending centered at a vertex atom. For example, R4 represents a C_2=C_3 stretching vibration, α1 represents a bending of the angle between the C_1=C_2 and C_1=C_6 bonds, and δC8 represents a bending vibration of the three C_8–H groups.

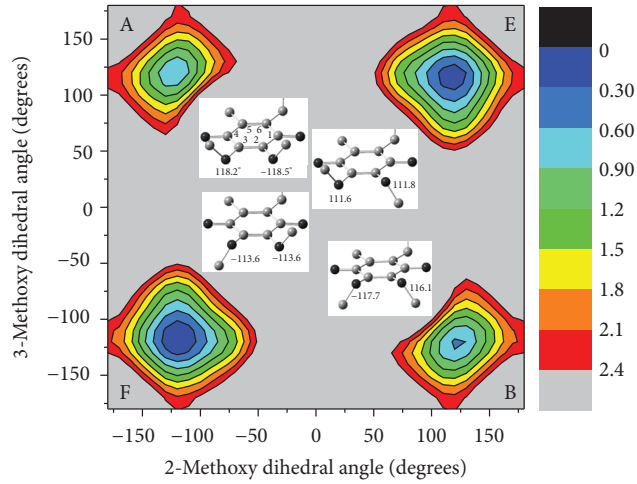

Figure 2: Calculated optimized energy (in kcal/mol) of UQ_1^- for all C_2 (C_3–C_2–O_{17}–C_9) and C_3 (C_4–C_3–O_{16}–C_8) dihedral angles. The energy axis was shifted so that the lowest energy conformer was set to zero. The insets show the structures of the four optimized methoxy group conformers (obtained for calculations in CCl_4). The emphasis is on displaying the methoxy group orientations, so hydrogen atoms have been removed and the tail at C_6 is not shown. Oxygen/carbon atoms are dark/light shade, respectively. C_2 and C_3 dihedral angles are also listed in each of the insets.

Table 1: Calculated bond lengths (in Å) and bond angles (in degrees) for all UQ_1^- conformers in the gas phase and CCl_4. Calculated methoxy group dihedral angles and relative energies (in kcal/mol) for all conformers are also listed. The lowest energy conformer is set to zero and the energies of UQ_1^- conformers relative to this zero are listed (kT at 298 K is ~0.59 kcal/mol). Bond lengths and angles for neutral UQ_{10} in the Q_A binding site (PDB file: 1AIJ) and UQ_{10}^- in the Q_B binding site (PDB file: 1AIG) are also listed.

	UQ_1^- in gas phase				UQ_1^- in CCl_4				Q_A	Q_B
	A	B	E	F	A	B	E	F		
$C_1\cdots O$	1.273	1.273	1.273	1.273	1.274	1.274	1.273	1.273	1.234	1.227
$C_4\cdots O$	1.272	1.272	1.271	1.271	1.247	1.274	1.274	1.274	1.232	1.221
$C_2\cdots C_3$	1.380	1.380	1.379	1.379	1.380	1.379	1.378	1.379	1.404	1.379
$C_5\cdots C_6$	1.384	1.384	1.384	1.384	1.384	1.385	1.385	1.385	1.419	1.398
C_6–C_{10}–C_{11}	113.4	113.5	113.5	113.5	113.3	113.2	113.3	113.2	113.0	111.0
C_3–C_2–O–CH_3	−121.8	120.8	116.7	−117.3	−118.5	116.1	111.8	−113.6	−57.1	79.9
C_2–C_3–O–CH_3	122.4	−123.2	118.3	−119.0	118.2	−117.7	111.6	−113.6	109.5	−121.3
ΔE	0.537	0.646	0.106	0	0.450	0.387	0.002	0		

similar to that found for UQ_{10}/UQ_{10}^- occupying the Q_A/Q_B binding site, respectively (Table 1).

3.3. Calculated Vibrational Frequencies of UQ_1^-. Figure 3(a) shows calculated IR spectra for the four UQ_1^- conformers in CCl_4, in the 1530–1425 cm^{-1} region. This spectral region is chosen because it is the region where the main C⋯O and C⋯C modes of UQ^- lie, and it is therefore the region generally focused upon in FTIR studies of UQ^- in solution [8–10]. The spectra of the conformers in Figure 3(a) have been scaled by the appropriate Boltzmann factors, which were calculated based on the relative energies of the four conformations (Table 1). A composite spectrum which is the sum of the four Boltzmann weighted spectra is also shown in Figure 3(a). The corresponding calculated composite spectra for UQ^- in various solvents are presented in Figures 3(b) and 3(c).

In the composite spectra an intense band is observed at 1500–1478 cm^{-1}, depending on the solvent. The frequency of this absorption band decreases, and the intensity increases, as the dielectric constant of the solvent increases. The frequency changes as a function of dielectric constant are outlined in the inset in Figure 3(a), which demonstrates that the band frequency is strongly solvent dependant only for solvents with dielectric constant ranging from ~1 to 20. Similar results have been found for PCM calculations of small neutral ketones in nonprotic solvents [22].

The calculated composite spectrum for UQ_1^- in CCl_4 (Figure 3(a)) displays an intense band at 1493 cm^{-1}. Lower intensity peaks are observed at 1483 and 1450 cm^{-1}. Table 2(b) lists the frequencies, IR intensities, Raman activities, and potential energy distributions for the normal modes that contribute to the bands in the spectra of UQ_{1F}^- in CCl_4. Similar results are calculated for conformers A, B, and E (data not shown), as would be expected given the similarity in the spectra of the conformers in Figure 3(a). For comparison, Table 2(a) also lists data for UQ_{1F}^- in the gas phase.

For UQ_1^- in CCl_4, the band at 1493 cm^{-1} (Figure 3(a)) is due to two intense normal modes at ~1491 and ~1495 cm^{-1}. The 1491 cm^{-1} normal mode is due predominantly to $C_4\cdots O$ stretching [R9(56%)] while the 1491 cm^{-1} normal mode is due predominantly to $C_1\cdots O$ stretching [R3(46%)]. For all four conformers, the $C_1\cdots O$ and $C_4\cdots O$ groups vibrate separately at a similar frequency with similar intensity. This is also observed for UQ_1^- in other solvents (not shown). This behavior is different from that found in calculations for neutral UQ_1, however, where most of the intensity is in only one of the C=O modes [21].

For UQ_1^- in the gas phase the most intense band is calculated at 1500 cm^{-1}. In gas phase calculations, however, this band is due to the out-of-phase vibration of both C⋯O groups [R3(29%)–R9(27%)] (Table 2(a)). In gas phase calculations, the in-phase vibration of both C⋯O groups is found at 1495 cm^{-1}, and it is approximately a factor of seven lower in intensity than the out-of-phase C⋯O vibration (Table 2(a)). In gas phase calculations the in-phase C⋯O vibration is very strongly Raman active while the out-of-phase C⋯O vibration is not. In contrast, for calculations in CCl_4, both the $C_1\cdots O$ and $C_4\cdots O$ vibrations are strongly Raman active.

In all spectra in Figure 3 a weak band is found at 1522 cm^{-1}. This band is due to an out-of-phase vibration of the C⋯C groups of the quinone ring (R4–R10). Given the antisymmetric nature of the vibration it is very weakly Raman active. The in-phase vibration of the C⋯C groups of the quinone ring occurs at 1607 cm^{-1} and is IR silent but very strongly Raman active (Table 2).

A relatively intense band is found at 1450–1456 cm^{-1} in all of the spectra in Figure 3. This band is due predominantly to CH bending vibrations of both methoxy methyl groups (δC8 and δC9) (Table 2(b)). Given that the mode is due to CH bending vibrations of the methoxy methyl groups it is not surprising that the precise frequency of this normal mode can vary by as much as 5 cm^{-1} among the four conformers (Figure 3(a)).

The calculated spectra of the four UQ_1^- conformers are similar (Figure 3(a)). We also find that the spectra are very similar for isotope-labeled versions of the conformers (not

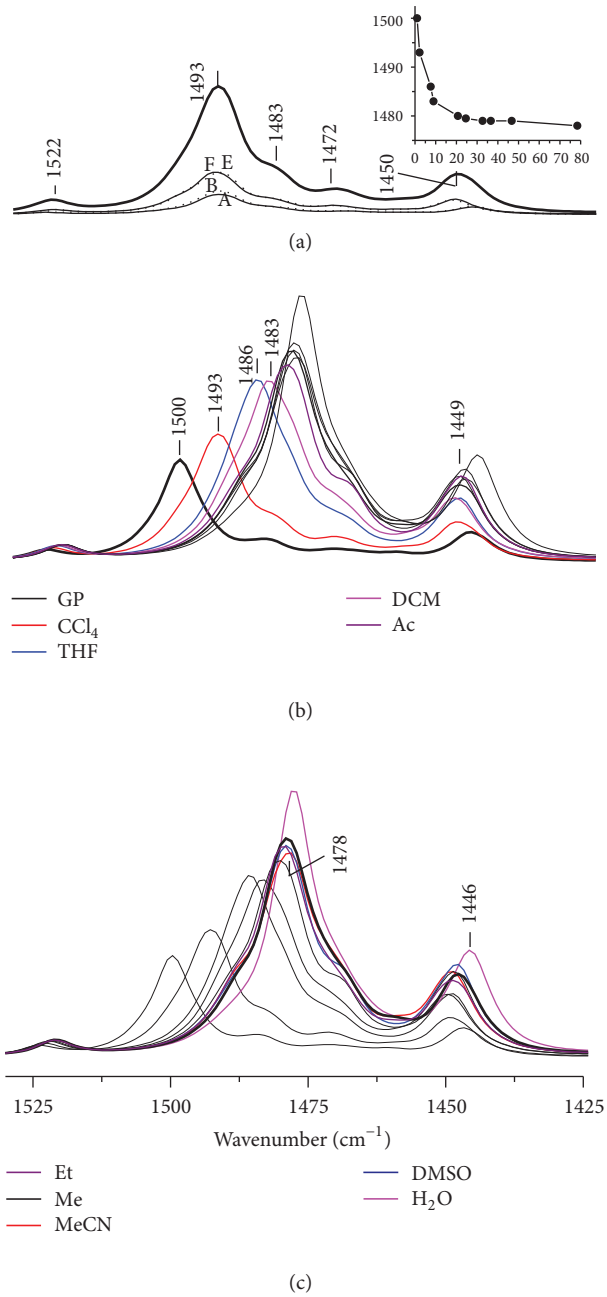

FIGURE 3: (a) Calculated Boltzmann weighted IR spectra for the four UQ_1^- conformations in CCl_4: UQ_{1A}^- and UQ_{1E}^- (*dotted*), UQ_{1B}^- and UQ_{1F}^- (*solid*). A composite spectrum that is the sum of the Boltzmann weighted spectra is also shown (thick line). (b) Calculated composite IR spectra for UQ_1^- in the gas phase (black), CCl_4 (red), THF (blue), DCM (magenta), and acetone (purple). (c) Calculated composite IR spectra for UQ_1^- in ethanol (purple), methanol (black), MeCN (red), DMSO (blue), and H_2O (magenta). The spectra displayed with thin lines in B/C are the spectra from C/B, respectively. All frequencies were scaled by 0.9808. *Inset:* graph of peak frequency as a function of solvent dielectric constant. Dielectric constants for CCl_4, THF, DCM, acetone, ethanol, methanol, acetonitryl, DMSO, and H_2O are 2.23, 7.58, 8.93, 20.7, 24.3, 32.63, 36.64, 46.7, and 78.39, respectively.

shown). For this reason we will consider only the Boltzmann weighted composite spectra below. In addition, we will consider spectra for UQ_1^- in CCl_4, noting that similar results and conclusions hold for UQ_1^- in other solvents.

Figure 4 shows calculated IR (*left*) and Raman (*right*) spectra for unlabeled, ^{13}C, and ^{18}O isotope-labeled UQ_1^- in the gas phase (a) and CCl_4 (b). The normal modes (frequencies, intensities, Raman activities, and PEDs) that give rise to the bands in the spectra in Figure 4 are also listed in Table 2.

As discussed above, for unlabeled UQ_1^- in CCl_4 the 1493 cm^{-1} band (IR spectrum) is due to separate $C_4\cdots O$ and $C_1\cdots O$ vibrations. Upon ^{13}C labeling the 1493 cm^{-1} band appears to downshift 39 cm^{-1} to 1454 cm^{-1} (Figure 4(b)). Such a downshift is expected for a band that is due to $C\cdots O$ groups. Table 2(b) indicates that the 1454 cm^{-1} band in the spectrum of ^{13}C labeled UQ_1^- in CCl_4 is due to a $C_4\cdots O$ stretching vibration mixed with CH methyl bending vibrations (associated with both methoxy methyl groups). A very low-intensity normal mode at 1458 cm^{-1} also contributes to the 1454 cm^{-1} band in the IR spectrum of ^{13}C-labeled UQ_1^- in CCl_4. This 1458 cm^{-1} mode is due to a $C_1\cdots O$ stretching vibration mixed with CH methoxy methyl bending vibrations (Table 2(b)). So both $C\cdots O$ groups give rise to intense normal modes for unlabeled UQ_1^- in CCl_4. However, upon ^{13}C labeling, only one intense $C\cdots O$ mode is found while the other is considerably weaker. Similar ^{13}C isotope-induced changes are found for calculations of UQ_1^- in the gas phase (Table 2(a)).

The band at 1449 cm^{-1} in the IR spectrum for unlabeled UQ_1^- in CCl_4 is due predominantly to CH bending vibrations of both methoxy methyl groups. Upon ^{13}C labeling the 1449 cm^{-1} band downshifts from 18 cm^{-1} to 1431 cm^{-1} (Figure 4(b)). The 1431 cm^{-1} mode is due to the out-of-phase vibration of both $C\cdots O$ groups [–R3(24%) + R9(11%)] coupled to a C_3 methoxy methyl bending vibration [δC8(32%)].

Other than the normal modes just discussed, $C\cdots O$ stretching vibrations (R9 and R3) contribute to at least 6 other modes in the 1500–1400 cm^{-1} region for ^{13}C-labeled UQ_1^-. Similar results are found for ^{13}C-labeled UQ_1^- in the gas phase.

In the IR spectrum of unlabeled UQ_1^- in CCl_4 the weak band at 1523 cm^{-1} is due predominantly to an out-of-phase $C\cdots C$ vibration (R4–R10). The in-phase $C\cdots C$ vibration (R4 + R10) occurs at 1607 cm^{-1}, with negligible IR intensity but high Raman activity (Figure 4(b)). The in-phase $C\cdots C$ mode downshifts 57 cm^{-1} to 1550 cm^{-1} upon ^{13}C labeling with little change in the mode composition (Table 2(b)).

In the unlabeled species the relatively pure $C\cdots O$ modes are found near 1493 cm^{-1} (in CCl_4). Upon ^{18}O labeling these $C\cdots O$ modes are expected to downshift from ~40 cm^{-1} to ~1453 cm^{-1}. In the unlabeled species the methoxy-methyl bending mode is found at 1450 cm^{-1}. So upon ^{18}O labeling the $C\cdots O$ modes and methyl bending modes will be similar in frequency and are therefore expected to strongly mix.

Table 2: Calculated vibrational frequencies (in cm^{-1}), intensities (in km/mol), Raman activities (in $Å^4$/amu), and potential energy distributions (%) of normal modes that contain contributions from C⋯O and/or C⋯C groups (R3, R9, R4, and R10) of unlabeled, ^{13}C-, and ^{18}O-labeled UQ_{1F}^- in (a) the gas phase and (b) CCl_4. Only contributions to the PED above 5% are considered. Frequencies are scaled by a factor 0.9808. For ^{18}O isotope labeling only the carbonyl oxygen atoms are labeled. R_i = ith bond stretching; δC_i = X–C_i–X bending for $–CH_3$, $–CH_2–$ and –CH= groups; X = atom bonded to C_i; RD1 = $6^{-1/2}(\alpha1 - \alpha2 + \alpha3 - \alpha4 + \alpha5 - \alpha6)$; RD2 = $12^{-1/2}(2\alpha1 - \alpha2 - \alpha3 + 2\alpha4 - \alpha5 - \alpha6)$ = ring deformation; α_i = C_{i-1}–C_i–C_{i+1} angle bending of ring atoms.

(a) Gas phase

ν	IR	Raman	Potential energy distribution
			Unlabeled
1448	94	5	R1(6) – R6(5) + δC8(26) + δC9(25)
1461	16	10	R3(9) – R10(5) + δC10(26) + δC7(31) + δC9(8)
1495	33	247	R9(34) + R3(22) – R10(10) + δC7(8)
1500	287	3	R3(29) – R9(27) + RD(9) + δC14(9)
1524	30	21	R4(33) – R10(16) – R5(6) – R7(6) + δC7(6)
1608	9	451	R4(26) + R10(23) + RD(12)
			^{13}C
1419	7	23	δC9(29) + δC8(22) + R4(12) – R10(11) + R3(6)
1430	218	6	δC8(35) – R3(20) + R9(8) + δC9(7)
1443	6	47	δC9(38) – R3(14) + R10(14) + δC7(7) – R9(6)
1458	13	61	R3(14) – R4(12) + δC9(10) + δC8(9) + R9(8) + δC7(6) + R10(6)
1459	195	25	R9(34) + δC8(22) + δC9(6) – RD1(6) – R10(5)
1474	8	130	δC8(32) + δC7(14) – R9(11) + δC9(20) – R3(6)
1481	23	23	δC14(37) + δC10(20) + δC13(13) + R3(7)
1519	34	18	δC7(33) – R4(15) + δC14(12) + δC13(5)
1550	7	384	R4(23) + R10(22) + RD2(11)
			^{18}O
1445	160	11	δC8(22) – R3(14) + δC9(12) + R1(8) – R6(6)
1455	11	53	R3(22) + δC9(21) + δC10(12) + δC7(8) – R10(6) + R9(5)
1466	10	33	δC14(24) + δC7(18) + δC13(16) + δC10(7) – R9(6)
1466	27	17	δC13(20) + δC7(19) + δC14(19) + R9(9)
1479	108	115	R9(37) + δC8(28)
1482	62	46	δC7(41) – R3(12) + δC14(5)
1486	46	33	δC13(57) + δC14(10) – R3(8)
1488	28	7	δC10(28) + δC13(23) + δC14(17) – R3(10)
1522	21	12	R4(31) – R10(20) + δC7(8) – R5(6) – R7(5)
1607	10	432	R4(27) + R10(24) + RD2(11)

(b) CCl_4

ν	IR	Raman	Potential energy distribution
			Unlabeled
1450	134	6	R3(5) – R1(5) + R6(5) + δC8(29) + δC9(23)
1460	17	11	R3(9) + δC10(28) + δC7(27) + δC9(9)
1491	184	328	R9(56) – R10(8)
1495	238	163	R3(46) + δC13(14) + RD1(6) + δC7(5) + δC9(5)
1523	36	27	R4(32) – R10(17) – R5(6) – R7(6) + δC7(6)
1607	11	869	R4(27) + R10(23) + RD2(12)
			^{13}C
1385	51	33	δC7(79) + R11(7) + R9(5)
1421	21	42	δC9(28) + δC8(18) – R10(13) + R4(11) + R3(9)
1431	365	7	δC8(32) – R3(24) + R9(11)
1443	15	91	δC9(39) + R10(14) – R9(12) – R3(11) + δC7(6)

(b) Continued.

ν	IR	Raman	Potential energy distribution
1454	243	48	R9(32) + δC8(27) + δC9(12) − RD1(6)
1458	17	156	R3(15) − R4(11) + δC9(8) + δC8(8) + R9(7) + R10(6) + δC7(12)
1474	7	190	δC9(38) + δC8(23) + δC7(11) − R3(6) − R9(6)
1479	27	34	δC13(39) + δC10(19) + δC14(14) + R3(6)
1487	39	16	δC7(28) + δC13(24) − R4(13) + δC14(5)
1549	9	752	R4(24) + R10(22) + RD2(11)
			^{18}O
1446	259	19	δC8(22) − R3(20) + R1(8) + δC9(6) − R6(6)
1455	9	101	δC9(24) − R3(17) + δC10(10) + R9(9) + δC7(8) + R10(6)
1465	97	131	R9(27) + δC7(18) + δC8(19)
1476	112	112	δC8(49) − R9(23)
1481	55	134	δC7(41) − R3(14) + δC9(10)
1483	52	49	δC14(52) + δC13(18) − R3(7)
1521	26	9	R4(30) − R10(21) + δC7(8) − R5(6) − R7(6)
1606	12	828	R4(28) + R10(24) + RD2(11)

Table 3: Calculated and experimental frequencies of selected normal modes of UQ^-. Isotope-induced frequency shifts are shown in parenthesis. Experimental Raman spectra have been obtained for UQ^- in the Q_A and Q_B binding sites, and for UQ^- in DCM. Calculated data are taken from Table 2(b).

Mode	Unlabeled			^{13}C			^{18}O	
	Calc	Raman[a]	FTIR[b]	Calc	Ramana	FTIR[b]	Calc	FTIR[b]
C⋯C(s)	1607	1605 Q_A 1613 Q_B 1607 (DCM)	—	1550(57)	1556(49) Q_A 1555(58) Q_B	—	1606(1)	
C⋯C(as)	1523	1523 Q_A 1532 Q_B 1521 (DCM)	—	1458(65) 1487(36)	1456(58) 1462(70)	—	1521(2)	
C⋯O	1491 1495	1486 Q_A 1489 Q_B 1489 (DCM)	1483	1454(37) 1458(37)	1456(30) 1462(27)	1442(41)	1476(15) 1465(26) 1481(14) 1483(12)	1468(15)

[a] Data from resonance Raman experiments [10]. [b] Data from FTIR experiments [8]. For ^{18}O isotope labeling only the carbonyl oxygen atoms are labeled.

Table 2(b) shows that upon ^{18}O labeling the C⋯O stretching vibrations do mix extensively with methyl bending vibrations, and that the C⋯O modes are distributed amongst at least five different mixed modes. From the IR spectra in Figure 4(b), one could argue that the 1493 cm^{-1} band downshifts from 18 cm^{-1} to 1475 cm^{-1} upon ^{18}O labeling. Such an ^{18}O isotope-induced frequency shift for semiquinones is in line with experimental observations [8, 23] (see below).

4. Discussion

The calculated changes in frequency, intensity, and mode composition upon isotope labeling of ubisemiquinone are considerably more complex than those found for the neutral species [21]. In spite of this, however, the calculated data allow a clear and detailed interpretation of bands in experimental Raman and FTIR spectra of ubisemiquinone. The calculated IR and Raman spectra presented in Figure 4(b) correspond very well to experimental spectra [8–10].

4.1. Modeling Isotope-Induced Bandshifts Observed in Resonance Raman Spectra. Resonance Raman spectra of unlabeled and ^{13}C-labeled UQ_{10}^- in the Q_A and Q_B binding sites in purple bacterial reaction centers have been obtained [10]. For comparison, resonance Raman spectra of unlabeled UQ_{10}^- in solution were also obtained [10]. For both *in vivo* and *in vitro* cases an intense Raman band was observed near 1608 cm^{-1}, with weaker bands observed near 1523 and 1488 cm^{-1}. We note that the calculated Raman spectrum for unlabeled UQ_1^- (Figure 4(b)) looks very similar to the experimental spectrum.

The ~1608 cm^{-1} band was assigned to a C⋯C mode, weakly coupled to a C⋯O mode, because it downshifted to 49–58 cm^{-1} upon ^{13}C labeling [10] (Table 3). The ~1488 cm^{-1} band was assigned to a C⋯O mode because it downshifted to ~28 cm^{-1} upon ^{13}C labeling [10] (Table 3). The ~1523 cm^{-1} band apparently disappears upon ^{13}C labeling. Although not suggested in the original manuscript, it is possible that the 1523 cm^{-1} band (of UQ_{10}^- in the Q_A

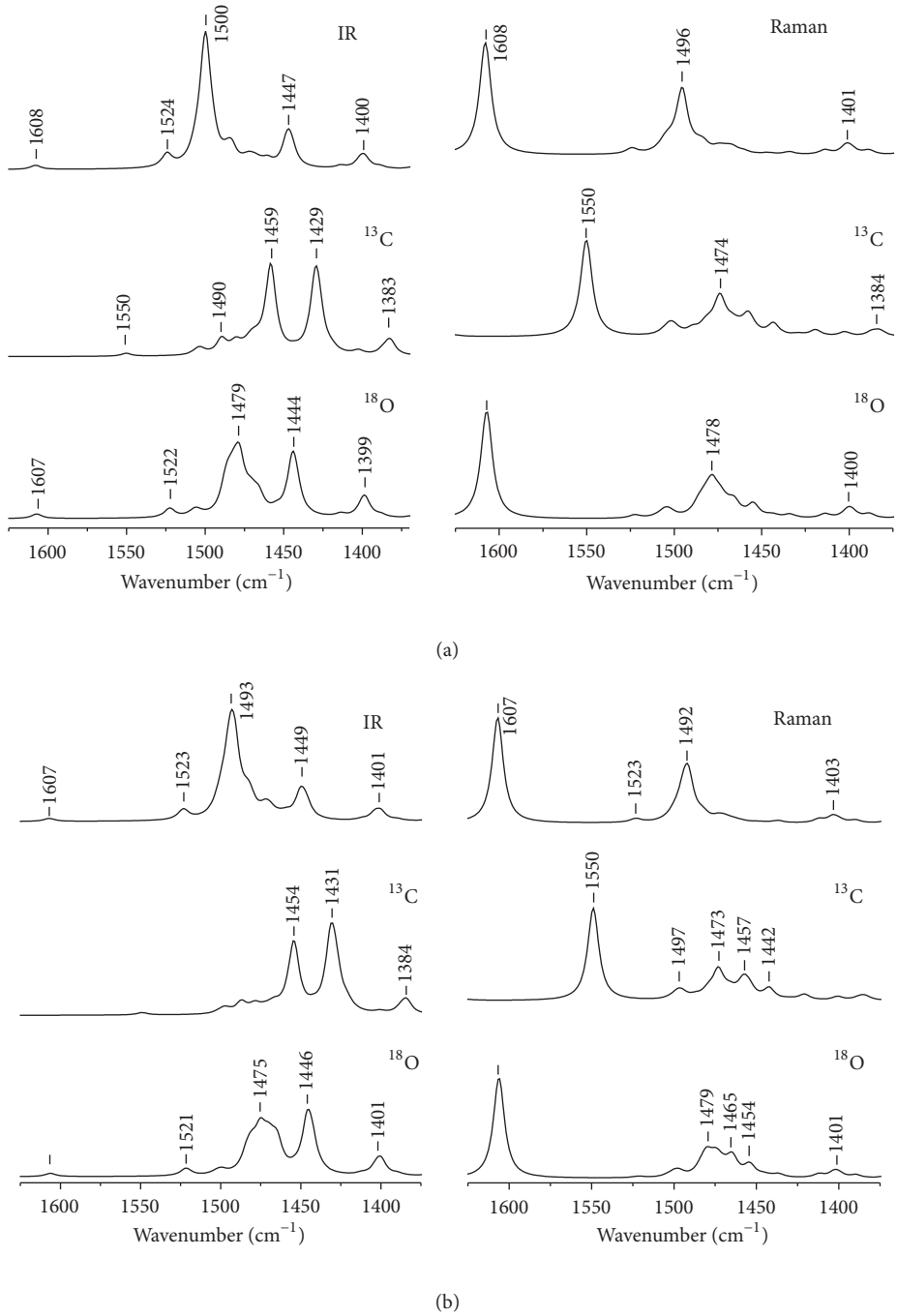

FIGURE 4: Calculated Boltzmann weighted composite IR (*left*) and Raman (*right*) spectra for unlabeled (*top*), ^{13}C (*middle*), and ^{18}O (*bottom*) labeled UQ_1^- in (a) the gas phase and (b) CCl_4. For ^{18}O isotope labeling only the carbonyl oxygen atoms are labeled.

binding site) downshifts from ~67 cm^{-1} to 1456 cm^{-1} upon ^{13}C labeling, and is masked by the ^{13}C⋯O band at 1456 cm^{-1} (Table 3).

In our calculations the $C_2\cdots C_3$ and $C_5\cdots C_6$ stretching vibrations couple to give C⋯C in-phase and out-of-phase vibrations. For UQ_1^- in CCl_4 the C⋯C in-phase vibration is at 1607 cm^{-1} (Figure 4(b)). This is 84 cm^{-1} higher in frequency than the out-of-phase vibration (at 1523 cm^{-1}). Unlike the out-of-phase vibration, the in-phase vibration is not coupled with methyl bending and carbonyl stretching modes (Table 2(b)). The C⋯C in-phase vibration has negligible IR intensity but huge Raman activity. It is basically unaffected by ^{18}O labeling, but downshifts to 57 cm^{-1} upon ^{13}C labeling. The intensely Raman active band calculated at 1607 cm^{-1} for UQ_1^- clearly corresponds to the band observed at ~1608 cm^{-1} experimentally [10].

The out-of-phase C⋯C vibrational mode at 1523 cm^{-1} mixes with other modes upon ^{13}C labeling and is not easily identifiable. A strongly Raman active mode of ^{13}C-labeled UQ^- is calculated at 1458 cm^{-1} (Table 2(b)). The out-of-phase C⋯C vibration contributes 17% to the PED of this mode [R10(6%)–R4(11%)]. The in-phase-coupled vibration of both C⋯O groups [R3(15%) + R9(7%)] also contributes to this mode.

Clearly, the calculated out-of-phase C⋯C vibrational mode at 1523 cm^{-1} can be associated with the band observed at ~1521 cm^{-1} in resonance Raman spectra of UQ^- in solution [10]. We suggest that the mode calculated at 1523 cm^{-1} forms part of a new mode that appears at 1458 cm^{-1} upon ^{13}C labeling (Table 3). In phase $^{13}C\cdots O$ vibrations also contribute to the 1458 cm^{-1} mode. Our calculated data therefore provides an explanation as to why the ~1521 cm^{-1} resonance Raman band that is observed experimentally is not identified in spectra of ^{13}C-labeled UQ^- [10]. Upon ^{13}C labeling the C⋯C mode mixes with C⋯O modes (and methyl bending modes) to become a new mode that is not distinctly identifiable as a $^{13}C\cdots{}^{13}C$ mode.

Bands at 1486/1489 cm^{-1} in resonance Raman spectra of UQ^- in the Q_A/Q_B binding site downshift 30/27 cm^{-1} upon ^{13}C labeling of UQ^- (Table 3), respectively. They were therefore associated with C⋯O modes coupled to C⋯C modes. Computationally, we find two C⋯O modes at 1495 and 1491 cm^{-1}. Both modes are Raman active with the 1491 cm^{-1} mode displaying the greater activity (Table 2(b)). These modes give rise to the 1492 cm^{-1} band in the calculated Raman spectrum (Figure 3(b)), which appears to downshift 19/35 cm^{-1} to 1473/1457 cm^{-1} upon ^{13}C-labeling. The 1473/1457 cm^{-1} band in the calculated Raman spectrum for ^{13}C labeled UQ_1^- is dominated by a mode at 1474/1458 cm^{-1}, respectively. The 1474 cm^{-1} mode and to a lesser degree the 1458 cm^{-1} mode are due predominantly to methyl CH bending vibrations of both methoxy groups coupled to a $C_1\cdots O$ vibration. Notice that the coupling of the $C_1\cdots O$ vibration is to methoxy methyl CH bending vibrations, *not* C⋯C ring vibrations, as was originally proposed based on the experimental spectra.

4.2. Modeling Isotope-Induced Bandshifts Observed in FTIR Spectra. Electrochemically generated FTIR difference spectra of UQ in various solvents have been obtained [8]. For UQ_{10}^- in acetonitrile, THF, or dichloromethane an intense FTIR absorption band was observed at 1483–1488 cm^{-1}. The observation of predominantly a single intense band in experimental FTIR spectra of unlabeled UQ_{10}^- and UQ_1^- in solution is in line with our calculated IR spectra, which are dominated by an intense band at 1478–1493 cm^{-1} for UQ_1^- in a variety of solvents (Figures 3(b) and 3(c)).

In experimental FTIR difference spectra for UQ_1^- in dichloromethane, a band is observed at 1483 cm^{-1}, which downshifts to 41 cm^{-1} upon ^{13}C labeling (Table 3) [8]. From Figure 3(b) it can be seen that upon ^{13}C labeling the 1493 cm^{-1} band downshifts from 39 cm^{-1} to 1454 cm^{-1}. The calculated result therefore agrees very well with the experimental observation.

Experimentally, for UQ_1^- in dichloromethane, it is also observed that the 1483 cm^{-1} band downshifts from 15 cm^{-1} to 1468 cm^{-1} upon ^{18}O labeling. From the calculated IR spectra in Figure 4(b), the most obvious suggestion is that the 1493 cm^{-1} band (of unlabeled UQ_1^-) downshifts from 18 cm^{-1} to 1475 cm^{-1} upon ^{18}O labeling. The calculated PEDs in Table 2(b) indicate a complicated situation: the 1495 and 1491 cm^{-1} modes of unlabeled UQ_1^- are due to the C⋯O groups (R3 and R9, resp.). Upon ^{18}O labeling modes appear at 1476 [R9(23%)] and 1465 cm^{-1} [R9(27%)]. Thus, the 1491 cm^{-1} mode in the unlabeled species appears to split and downshift to 15 and 26 cm^{-1} upon ^{18}O labeling (Table 3). The former is in excellent agreement with experiment [8]. Upon ^{18}O labeling modes also appear at 1481 [R3(14%)] and 1483 cm^{-1} [R3(7%)]. Thus, the 1495 cm^{-1} mode in the unlabeled species also appears to split and downshift to 14 and 12 cm^{-1} upon ^{18}O labeling (Table 3). Again, these conclusions are in good agreement with experiment [8]. It is the plethora of mixed modes that appear upon ^{18}O labeling that give rise to the broad band with a peak near 1475 cm^{-1} in the calculated spectrum (Figure 3(b)). Unfortunately FTIR spectra for ^{18}O-labeled UQ_1^- have never been presented. Only the observed shifts upon labeling were presented.

From electrochemically generated FTIR difference spectra of ^{13}C-labeled UQ_{10}^- in various solvents [8] a band was observed at 1412 cm^{-1}. It was suggested that this band was due to a $^{13}C\cdots{}^{13}C$ vibration that was downshifted to 71 cm^{-1} from 1483 cm^{-1} in the unlabeled species. Neither the calculated data presented here nor the resonance Raman data presented previously support this hypothesis.

4.3. Experimental Q_A^-/Q_A and Q_B^-/Q_B FTIR DS. Q_A^-/Q_A and Q_B^-/Q_B FTIR DS have been obtained using PBRCs from *R. sphaeroides* [7, 24–27]. In Q_A^-/Q_A FTIR DS three intense IR bands are observed near 1485, 1466, and 1449 cm^{-1} [24, 25]. On the basis of ^{18}O, ^{13}C, $^{13}C_1$, and $^{13}C_4$ labeling the 1486/1466 cm^{-1} bands were assigned to C⋯O/C⋯C vibrations, respectively [24]. The modes were suggested to be considerably mixed. The origin of the 1449 cm^{-1} band was not considered.

Another group, which undertook identical labeling experiments [25], assigned the 1485 cm^{-1} band to a $C_1\cdots O$ vibration, the 1466 cm^{-1} band to C_4=O vibration, and the 1449 cm^{-1} band to a C⋯C vibration. All modes were suggested to be strongly mixed.

Resonance Raman spectra for UQ^- in the Q_A binding site display a weak band at 1486 cm^{-1}, but no bands were apparent at 1466 and 1449 cm^{-1}. Of course it may simply be the case that the 1466 and 1449 cm^{-1} normal modes are Raman inactive.

Our calculated spectra for UQ_1^- in solution poorly model observed FTIR bands of UQ^- in the Q_A binding site. For UQ^-

in the Q_A binding site, the C⋯O modes appear to be separated by 19 cm^{-1}. For calculations in solvent the two C⋯O modes do appear to be distinct, although the separation of the modes is only 4 cm^{-1}. In gas phase calculations the two C⋯O modes are coupled. The separation of C⋯O modes of UQ^- in the Q_A binding site is due to asymmetric interactions with the protein environment. Calculations of UQ^- in solvent or in the gas phase cannot model these interactions. Calculations including effects of the protein environment are essential. Such calculations are underway in our lab.

In Q_B^-/Q_B FTIR DS a single IR band is observed near 1479 cm^{-1}. It was suggested that this band was due to both C⋯O modes of UQ^- in the Q_B binding site [7, 26, 27]. It was also suggested that the 1479 cm^{-1} band downshifts 33/52 cm^{-1} upon $^{18}O/^{13}C$ labeling, respectively [7, 26, 27]. Such shifts are difficult to rationalize in view of the shifts calculated (15/37 cm^{-1}) and observed experimentally (15/27–41 cm^{-1}) for UQ in solution (Table 3). Additionally, there appears to be some inequivalence in the C⋯C modes of UQ in the Q_B binding site when perturbed specifically at the C_1 or C_4 position [7, 26, 27]. It was suggested that this inequivalence is a result of specific protein interactions [7, 26, 27]. Again, calculations including effects of the protein environment appear to be necessary (essential) in order to accurately simulate the vibrational spectra of UQ in the Q_B binding site.

4.4. Previous Calculations of Ubisemiquinones. DFT-based vibrational frequency calculations (using the BP86 functional) have been undertaken for 2,3-dimethoxy-1,4-benzoquinone and 2,3-dimethoxy-5,6-dimethyl-1,4-benzoquinone in the gas phase [12]. Comparison of calculated data for the two models showed that substituents at C_5 and C_6 are required in order to better model the properties of ubiquinones and ubisemiquinones. In the above study isotope shifts were calculated. However how the C⋯O and C⋯C modes couple with each other and with CH methoxy methyl bending vibrations was not considered. As we have shown above, the extent of mode mixing can be considerably altered upon labeling, making it difficult to identify how the different bands shift upon labeling. As we show here, the detailed PEDs are a crucial tool in the analysis of how calculated bands shift upon isotope labeling.

One problem with previous DFT calculations (in the gas phase) [12] is that for 2,3-dimethoxy-1,4-benzoquinone the C⋯O modes were found at a higher frequency than the C⋯C modes. For 2,3-dimethoxy-5,6-dimethyl-1,4-benzoquinone (in the gas phase) the C⋯O modes were found at slightly lower frequency than the C⋯C modes (3-4 cm^{-1}). However, from Raman experiments the out-of-phase C⋯C mode is found to be ~32 cm^{-1} higher in frequency than the C⋯O mode [10] (Table 3).

Furthermore, the antisymmetrically coupled C⋯O mode (for 2,3-dimethoxy-5,6-dimethyl-1,4-benzoquinone) was calculated to be more than a factor of 26 times more intense than the C⋯C mode [12]. This calculated result is not in line with experimental IR spectra [8].

Clearly, previous DFT calculations [12] poorly model the experimental Raman and IR spectra. In contrast, in our calculations for UQ_1^- in CCl_4, the out-of-phase C⋯C modes are 28–32 cm^{-1} higher in frequency than either of the C⋯O mode (Table 2(b)). In gas phase calculations the out-of-phase C⋯C mode is still 24 cm^{-1} higher in frequency than the antisymmetrically coupled C⋯O mode (Table 2(a)). In addition, in gas phase calculations and in solvent, the intensity of antisymmetrically coupled C⋯O mode is ~7.5 times more intense than the out-of-phase C⋯C mode. These results are in excellent agreement with experimental IR and Raman spectra. The limitations in previous calculations are most likely related to the choice of functional and basis set, and the inadequacy of a UQ structural model that lacks an isoprene unit.

5. Conclusions

We calculate that four UQ_1^- conformers are likely present in solution at room temperature. Calculated IR spectra for all four UQ_1^- conformers are similar. Calculated IR spectra of unlabeled and isotope-labeled UQ_1^- in the gas phase and in solution show a similar band pattern, although in some cases there are differences in the composition of the modes that contribute to the bands in the spectra.

Calculations show that upon isotope labeling the out-of-phase C⋯C ring modes and C⋯O modes of UQ_1^- strongly couple with methyl C–H bending vibrations of the methoxy groups. This leads to complicated splitting of modes and unusual downshifts upon isotope labeling. Nonetheless by consideration of PEDs of the calculated normal modes, sense can be made of the isotope-induced shifts and intensity changes, and it is shown that the calculated data provide a rational and detailed interpretation of experimentally observed isotope-induced band shifts in experimental FTIR and Raman spectra of UQ_1^- in solution.

Abbreviations

DFT: Density functional theory
DS: Difference spectra
FTIR: Fourier transform infrared
IR: Infrared
IEF: Integral equation formalism
PBRCs: Purple bacterial reaction centers
PCM: Polarizable continuum model
PED: Potential energy distribution
UQ: Ubiquinone
UQ^-: Ubisemiquinone.

Acknowledgments

H. P. Lamichhane acknowledge support from a fellowship from the Molecular Basis of Disease Program at Georgia State University. G. Hastings acknowledges the support from Qatar National Research Fund.

References

[1] B. Trumpower, *Function of Quinones in Energy Conserving Systems*, Academic Press, 1982.

[2] B. Ke, "The bacterial photosynthetic reaction center: chemical composition and crystal structure," in *Photosynthesis: Photobiochemistry and Photobiophysics*, pp. 47–62, Kluwer Academic Publishers, Dordrecht, The Netherlands, 2001.

[3] B. Ke, "The, "Stable" primary electron acceptor (Q_A) of photosynthetic bacteria," in *Photosynthesis: Photobiochemistry and Photobiophysics*, pp. 101–110, Kluwer Academic Publishers, Dordrecht, The Netherlands, 2001.

[4] B. Ke, "The secondary electron acceptor (Q_B) of photosynthetic bacteria," in *Photobiochemistry and Photobiophysics*, pp. 111–128, Kluwer Academic Publishers, Dordrecht, The Netherlands, 2001.

[5] N. Srinivasan and J. H. Golbeck, "Protein-cofactor interactions in bioenergetic complexes: the role of the A1A and A1B phylloquinones in Photosystem I," *Biochimica et Biophysica Acta*, vol. 1787, no. 9, pp. 1057–1088, 2009.

[6] C. A. Wraight and M. R. Gunner, "The acceptor quinones of purple photosynthetic Bacteria-structure and spectroscopy," in *The Purple Photosynthetic Bacteria*, C. N. Hunter, F. Daldal, M. C. Thurnauer, and J. T. Beatty, Eds., pp. 379–405, Springer, 2009.

[7] J. Breton and E. Nabedryk, "Protein-quinone interactions in the bacterial photosynthetic reaction center: light-induced FTIR difference spectroscopy of the quinone vibrations," *Biochimica et Biophysica Acta*, vol. 1275, no. 1-2, pp. 84–90, 1996.

[8] M. Bauscher and W. Mäntele, "Electrochemical and infrared-spectroscopic characterization of redox reactions of p-quinones," *Journal of Physical Chemistry*, vol. 96, no. 26, pp. 11101–11108, 1992.

[9] M. Bauscher, E. Nabedryk, K. Bagley, J. Breton, and W. Mantele, "Investigation of models for photosynthetic electron acceptors. Infrared spectroelectrochemistry of ubiquinone and its anions," *FEBS Letters*, vol. 261, no. 1, pp. 191–195, 1990.

[10] X. Zhao, T. Ogura, M. Okamura, and T. Kitagawa, "Observation of the resonance raman spectra of the semiquinones QA·- and QB·- in photosynthetic reaction centers from *Rhodobacter sphaeroides* R26," *Journal of the American Chemical Society*, vol. 119, pp. 5263–5264, 1997.

[11] G. Balakrishnan, P. Mohandas, and S. Umapathy, "Ab initio studies on structure and vibrational spectra of ubiquinone and its radical anion," *Spectrochimica Acta A*, vol. 53, no. 10, pp. 1553–1561, 1997.

[12] M. Nonella, "A density functional investigation of model molecules for ubisemiquinone radical anions," *Journal of Physical Chemistry B*, vol. 102, no. 21, pp. 4217–4225, 1998.

[13] M. J. Frisch, G. W. Trucks, H. B. Schlegel et al., 2004.

[14] K. M. Bandaranayake, V. Sivakumar, R. Wang, and G. Hastings, "Modeling the A1 binding site in photosystem. I. Density functional theory for the calculation of "anion—neutral" FTIR difference spectra of phylloquinone," *Vibrational Spectroscopy*, vol. 42, no. 1, pp. 78–87, 2006.

[15] E. Cancès, C. Le Bris, B. Mennucci, and J. Tomasi, "Integral equation methods for molecular scale calculations in the liquid phase," *Mathematical Models and Methods in Applied Sciences*, vol. 9, no. 1, pp. 35–44, 1999.

[16] E. Cancès, B. Mennucci, and J. Tomasi, "A new integral equation formalism for the polarizable continuum model: theoretical background and applications to Isotropic and anisotropic dielectrics," *Journal of Chemical Physics*, vol. 107, no. 8, pp. 3032–3041, 1997.

[17] J. Tomasi, B. Mennucci, and E. Cancès, "The IEF version of the PCM solvation method: an overview of a new method addressed to study molecular solutes at the QM ab initio level," *Journal of Molecular Structure*, vol. 464, no. 1–3, pp. 211–226, 1999.

[18] J. Tomasi, R. Cammi, B. Mennucci, C. Cappelli, and S. Corni, "Molecular properties in solution described with a continuum solvation model," *Physical Chemistry Chemical Physics*, vol. 4, no. 23, pp. 5697–5712, 2002.

[19] J. Tomasi, B. Mennucci, and R. Cammi, "Quantum mechanical continuum solvation models," *Chemical Reviews*, vol. 105, no. 8, pp. 2999–3093, 2005.

[20] J. M. L. Martin and C. Van Alsenoy, *GAR2PED*, University of Antwerp, 1995.

[21] H. Lamichhane, R. Wang, and G. Hastings, "Comparison of calculated and experimental FTIR spectra of specifically labeled ubiquinones," *Vibrational Spectroscopy*, vol. 55, no. 2, pp. 279–286, 2011.

[22] C. Cappelli, C. O. Silva, and J. Tomasi, "Solvent effects on vibrational modes: ab-initio calculations, scaling and solvent functions with applications to the carbonyl stretch of dialkyl ketones," *Journal of Molecular Structure*, vol. 544, pp. 191–203, 2001.

[23] G. Hastings, K. M. P. Bandaranayake, and E. Carrion, "Time-resolved FTlR difference spectroscopy in combination with specific isotope labeling for the study of A1, the secondary electron acceptor in photosystem 1," *Biophysical Journal*, vol. 94, no. 11, pp. 4383–4392, 2008.

[24] J. Breton, J. R. Burie, C. Berthomieu, G. Berger, and E. Nabedry, "The binding sites of quinones in photosynthetic bacterial reaction centers investigated by light-induced FTIR difference spectroscopy: assignment of the Q_A vibrations in *Rhodobacter sphaeroides* using ^{18}O- $Or^{13}C$-labeled ubiquinone and vitamin K_1," *Biochemistry*, vol. 33, no. 16, pp. 4953–4965, 1994.

[25] R. Brudler, H. J. M. De Groot, W. B. S. Van Liemt et al., "Asymmetric binding of the 1- and 4- C = O groups of Q_A in *Rhodobacter sphaeroides* R26 reaction centres monitored by Fourier transform infra-red spectroscopy using site-specific isotopically labelled ubiquinone-10," *EMBO Journal*, vol. 13, no. 23, pp. 5523–5530, 1994.

[26] J. Breton, C. Boullais, G. Berger, C. Mioskowski, and E. Nabedryk, "Binding sites of quinones in photosynthetic bacterial reaction centers investigated by light-induced FTIR difference spectroscopy: symmetry of the carbonyl interactions and close equivalence of the QB vibrations in *Rhodobacter sphaeroides* and Rhodopseudomonas viridis probed by isotope labeling," *Biochemistry*, vol. 34, no. 36, pp. 11606–11616, 1995.

[27] R. Brudler, H. J. M. De Groot, W. B. S. Van Liemt et al., "FTIR spectroscopy shows weak symmetric hydrogen bonding of the Q_B carbonyl groups in *Rhodobacter sphaeroides* R26 reaction centres," *FEBS Letters*, vol. 370, no. 1-2, pp. 88–92, 1995.